Journal Pre-proof

A new chitosan-based thermosensitive nanoplatform for combined photothermal and chemotherapy

Yanyan Zhang, Gareth R. Williams, Jiadong Lou, Wanting Li, Cuiwei Bai, Tong Wang, Shiwei Niu, Chun Feng, Li-Min Zhu

PII: S0141-8130(22)02626-5

DOI: https://doi.org/10.1016/j.ijbiomac.2022.11.068

Reference: BIOMAC 22522

To appear in: *International Journal of Biological Macromolecules*

Received date: 8 September 2022

Revised date: 30 October 2022

Accepted date: 8 November 2022

Please cite this article as: Y. Zhang, G.R. Williams, J. Lou, et al., A new chitosan-based thermosensitive nanoplatform for combined photothermal and chemotherapy, *International Journal of Biological Macromolecules* (2022), https://doi.org/10.1016/j.ijbiomac.2022.11.068

A new chitosan-based thermosensitive nanoplatform for combined photothermal and chemotherapy

Yanyan Zhang[a], *Gareth R. Williams*[b], *Jiadong Lou*[a], *Wanting Li*[c], *Cuiwei Bai*[c], *Tong Wang*[a], *Shiwei Niu*[c], *Chun Feng*[d,*], *Li-Min Zhu*[a,*]

[a]College of Biological Science and Medical Engineering, Shanghai Engineering Research Center of Nano-Biomaterials and Regenerative Medicine, Donghua University, Shanghai 201620, PR China

[b]UCL School of Pharmacy, University College London, 29-39 Brunswick Square, London, WC1N 1AX, UK

[c]Yunnan Key Laboratory of Stem Cell and Regenerative Medicine, Science and Technology Achievement Incubation Center, Kunming Medical University, Kunming 650500, PR China

[d]Department of Otolaryngology, the First People's Hospital of Yunnan Province, the Affiliated Hospital of Kunming University of Science and Technology, Kunming 650032, PR China

*Corresponding authors:dt0874@163.com (C. Feng), lzhu@dhu.edu.cn (L.-M. Zhu).

Abstract:

Targeting the delivery of anti-cancer drugs to a tumor site is essential for effective treatment and to ensure minimal damage to healthy cells and tissues. In this work, a chitosan-based nanoplatform was constructed for combined photothermal therapy and chemotherapy of breast cancer. The pH-sensitive and biocompatible biopolymer chitosan (CS) was grafted with *N*-vinylcaprolactam (NVCL) and modified with biotin (Bio), imparting it with temperature sensitive property and the ability of active targeting. The polymer self-assembled to give nanoparticles (NPs) loaded with indocyanine green (ICG) and doxorubicin (DOX). When the NPs are exposed to near-infrared (NIR) laser irradiation, ICG converts the light to heat, inducing a significant phase transition in NPs and facilitating the release of the drug cargo. In addition, the solubility of chitosan is increased in the slightly acidic microenvironment of the tumor site, which also promotes drug release. A detailed

analysis of the NPs both in vitro and in vivo showed that the carrier system is biocompatible, while the drug-loaded NPs are selectively taken up by cancer cells. Particularly when augmented with NIR irradiation, this leads to potent cell death in vitro and also in an in vivo murine xenograft model of breast cancer.

Keywords: Photothermal therapy, Chitosan, Thermosensitive material

1. Introduction

Breast cancer, which commonly results in malignant tumors, remains a serious threat to women's health [1-4]. Chemotherapy is widely used as a first-line treatment [5, 6], but suffers from a number of drawbacks. The active pharmaceutical ingredients (APIs) used frequently have poor water solubility and are non-specific (affecting healthy tissues as well as the tumor), which results in systemic toxicity [7]. As a result, numerous nanocarriers have emerged to improve the efficiency of chemotherapy. Nanoparticles (NPs) can passively target tumors through the enhanced permeability and retention (EPR) effect, and active targeting can be achieved by modifying the NPs with targeting ligands [8-10]. Further, NPs can be designed to release their API cargo in response to an internal or external stimulus [11, 12]. Internal stimuli are mainly based on the characteristics of the tumor microenvironment [13, 14], such as its slight acidity and high temperature, while appropriate external stimulation includes near infrared (NIR) laser irradiation and ultrasound, among others [15, 16].

Chitosan, a natural polymer, has attracted significant attention as a nanocarrier for anti-cancer APIs. This is because it has a number of advantageous properties, including antimicrobial activity [17, 18], good biocompatibility, biodegradability and pH sensitivity [19, 20]. Chitosan is frequently grafted with thermosensitive materials to build dual-responsive nanocarriers [21-23]. These temperature-sensitive materials are designed to release an API cargo more rapidly at the slightly higher temperature of the tumor microenvironment (cf. the standard physiological temperature). Zhang et al. developed a dual-responsive drug delivery system comprising chitosan and the temperature-responsive material di(ethylene glycol) methyl ether methacrylate and employed this to deliver paclitaxel for enhanced breast cancer therapy [24]. Similarly, Chen and co-workers constructed nanocomposites based on thermosensitive

poly(*N*-vinylcaprolactam) and chitosan to realize co-delivery of doxorubicin and oleanolic acid for cancer chemotherapy [25]. These NPs respond to the slightly higher temperature at the tumor site, but the temperature of the tumor is only 1-2 °C greater than that of the normal tissues [26]. This makes it difficult to achieve accurate targeting based on the endogenous difference in temperature alone. To improve targeting, a photothermal agent can be incorporated with a temperature-sensitive material. The aim here is to use the sensitizer to absorb light (particularly NIR, which has good tissue penetration properties) and use this to generate a large amount of local heating via photothermal conversion. Compared with NPs that respond to endogenous temperature differences [24, 25], this system can more effectively induce a phase transition via photothermal agent in the temperature-sensitive component and thus release the API in a targeted manner.

The heat generated via a photothermal agent can also be used to directly ablate tumor tissue in a process termed photothermal therapy (PTT). This approach has been widely explored for tumor treatment by virtue of its having a number of advantages: it has deep tissue penetration, is noninvasive, safe and allows high spatiotemporal resolution [27-30]. Indocyanine green (ICG), a fluorescent dye, is a promising photothermal agent approved by the Food and Drug Administration (FDA) for human clinical applications [31-33]. Due to its excellent photothermal conversion ability ICG has gained much attention, but it suffers from similar challenges to chemotherapeutic drugs in that its distribution is non-specific and it has a short blood circulation time [34-36].

To precisely target chemotherapeutic APIs or photothermal agents and avoid damage to healthy tissues and cells, suitable tumor-targeting ligands can be attached to NPs [37-39]. Biotin is one suitable ligand. It is an essential micronutrient for cell proliferation [40, 41], and its receptor, sodium-dependent multivitamin transporter, is overexpressed on the surfaces of numerous cancer cell membranes, including those of breast cancer cells and human cervical cancer cells [42-45]. Moreover, biotin is a small molecule with advantages of low cytotoxicity and no inherent immunogenicity [46].

In this work, we developed a chitosan-based nanoplatform to accomplish combined PTT and chemotherapy for breast cancer. Chitosan was grafted with temperature-sensitive *N*-vinylcaprolactam (NVCL) and the composite was modified with biotin to provide tumor-targeting. The hydrophobic chemotherapy API doxorubicin (DOX) and photothermal agent ICG were co-loaded in the core of NPs through self-assembly to yield the DOX/ICG@Bio-CS-PNVCL system. After accumulation at the tumor site, under NIR irradiation the ICG should generate heat, raising the local temperature at the tumor for PTT and also stimulating DOX release from the NPs. Furthermore, the enhanced solubility of chitosan under the acidic conditions in the tumor also promotes the release of DOX. This should result in effective, targeted, dual-mode cancer therapy. The approach is summarized in Scheme 1.

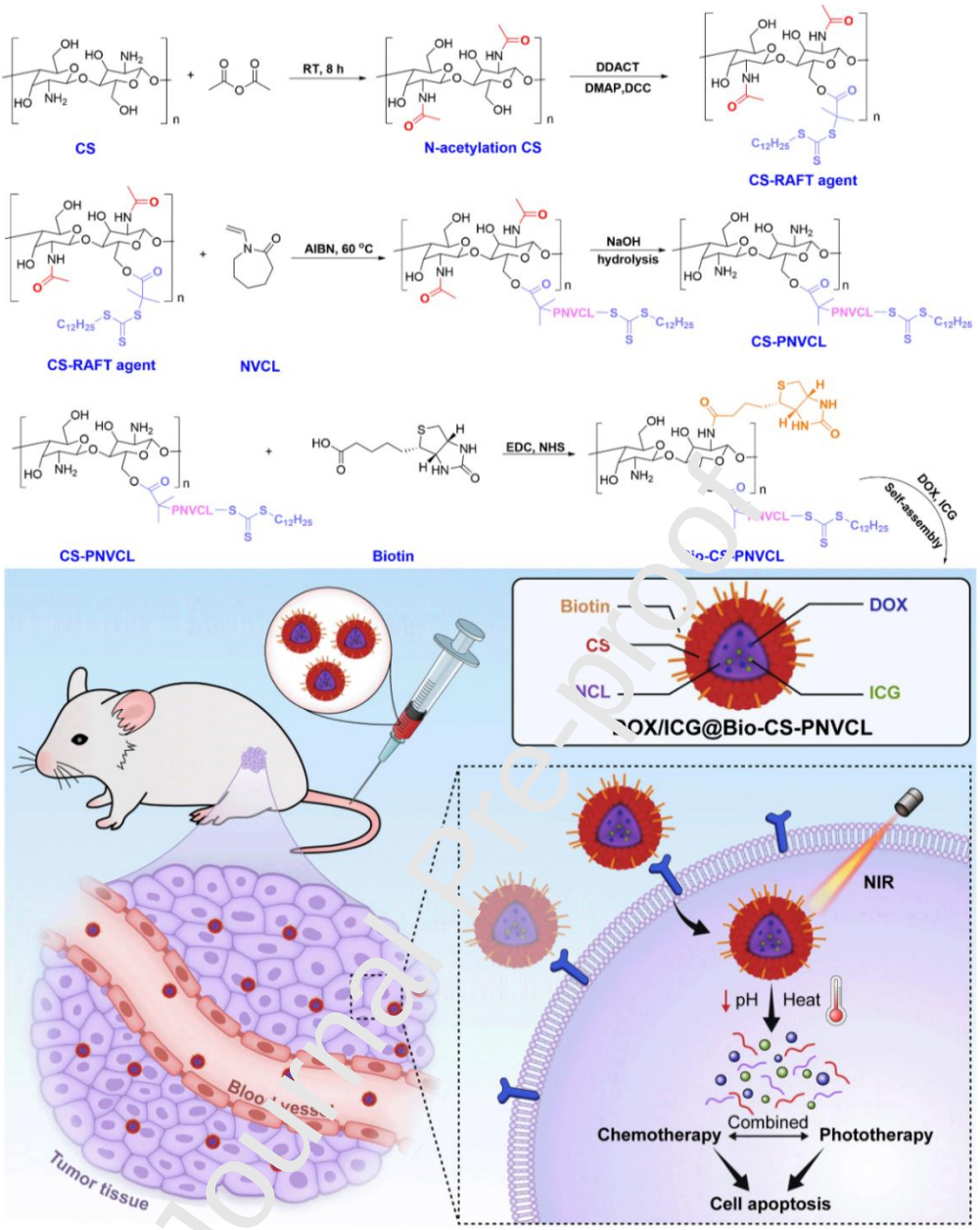

Scheme 1 Schematic illustration of the chitosan-based DOX/ICG@Bio-CS-PNVCL NPs developed in this work for NIR laser triggered PTT-chemotherapy.

2. Materials and methods

2.1 Materials

Chitosan (degree of deacetylation = 90%), *N*-hydroxysuccinimide (NHS) and 2,2'-azobis(2-methylpropionitrile) (AMPN) were sourced from Macklin Biochemical Co., Ltd. Acetic acid came from Tianjin Fengchuan Chemical Reagent Technologies Co., Ltd. Biotin (Bio) and acetic anhydride was purchased from Sinopharm Chemical

Reagent Co., Ltd. Doxorubicin (DOX) was sourced from Shanghai Haohong Biomedical Technology Co., Ltd. Indocyanine green (ICG), 2-(dodecyltrithiocarbonate)-2-methylpropionic acid (DDACT), DMSO-d_6 and D_2O were provided by Shanghai Yishi Chemical Co., Ltd. *N*-Vinylcaprolactam (NVCL) was obtained from Bentong (Shanghai) Chemical Co., Ltd. *N*,*N*-Dimethylformamide (DMF), *N*,*N'*-dicyclohexylcarbodiimide (DCC) and 4-dimethylaminopyridine (DMAP) was procured from Shanghai Aladdin Biochemical Technology Co., Ltd. Dialysis bags and 1-(3-dimethylaminopropyl)-3-ethylcarbodiimide hydrochloride (EDC) were obtained from Shanghai Yuanye Bio-Technology Co., Ltd.

4T1 cells and L929 cells were provided by Procell Life Science & Technology Co., Ltd. Dulbecco's Modified Eagle Medium (DMEM) and phosphate-buffered saline (PBS) were sourced from Corning. Fetal bovine serum (FBS) was provided by Biological Industries Israel Beit Haemek Ltd. Methyl thiazolyl tetrazolium (MTT) was supplied by Shanghai Yeasen Biotechnology Co., Ltd. A Calcein-AM/PI double staining kit (AM/PI) was obtained from Life Technologies Corporation. DAPI staining solution was procured from Beijing Labgic Technology Co., Ltd. Penicillin-streptomycin (pen-strep) solution was sourced from Biological Industries. Trypsin-EDTA (0.25%) was provided by the Life Technologies Corporation. A hematoxylin and eosin (H&E) staining kit, terminal deoxynucleotidyl transferase-mediated dUTP nick-end labeling (TUNEL) apoptosis assay kit and Ki67 cell proliferation kit were purchased from Sigma-Aldrich Co., Merck KgaA and Abcam Co., respectively.

Female nude mice aged 5-6 weeks were provided by the Animal Center of Kunming Medical University. All animal experiments were performed following review and approval by the Animal Care and Use Committee of Kunming Medical University (ref: KMMU 2015002). All animal care and handling protocols were carried out according to the Guideline for the Care and Use of Laboratory Animals published by the US National Institutes of Health (NIH Publication No. 8523, revised in 1985).

2.2 Preparation of Bio-CS-PNVCL

CS (1 g) was dissolved in aqueous acetic acid solution (1.0% v/v, 100 mL) containing acetic anhydride (0.4 mL). Subsequently, ethanol (100 mL) was added and reaction carried out at room temperature for 8 h. Next, the mixture was poured into a mixture of water and ethanol (500 mL, v/v=1:4), and soon afterwards a precipitate emerged. The precipitate was collected by centrifugation, washed with ultrapure water, re-precipitated with the water/ethanol mixture, and finally collected by centrifugation. These steps were repeated three times. Finally, the obtained product was dried under vacuum at room temperature for 2 hours to acquire pure N-acetylated CS (N-CS).

N-CS (290 mg) was added into DMF (30 mL). DCC (205 mg), DMAP (15 mg) and DDACT (370 mg) were added in sequence, with a pause between each addition until complete dissolution had occurred. Subsequently, the mixture was stirred at room temperature for 48 hours. The reaction solution was then dropped into ice water and a yellow solid emerged. This suspension of yellow solid was put into a dialysis bag (MWCO 3500Da) and dialyzed with double distilled water for three days. The collected product was freeze-dried to obtain CS-RAFT.

CS-RAFT (50 mg) was dissolved in DMF (5 mL) under the protection of nitrogen, followed by adding AMPN (9.6 mg) and NVCL (1 g). The mixture was stirred at 60 ^{o}C for 24 h. After cooling to room temperature, the solution was poured into ice water and dialyzed in dialysis bags (MWCO 3500 Da) with double distilled water for three days. CS-PNVCL was obtained by freezing and drying. CS-PNVCL (30 mg) was then dissolved in aqueous NaOH solution (10% NaOH w/w, 10 mL) and stirred at room temperature. After 48 hours deprotected CS-PNVCL was obtained by dialysis, and freeze dryied as above.

Deprotected CS-PNVCL (50 mg) was dissolved in DMF (15 mL), followed by addition of EDC (50 mg) and NHS (30 mg). The solution was stirred at room temperature for 2 hours to activate the amino group. Biotin (50 mg) was then added and the reaction mixture was stirred for a further 24 hours to produce Bio-CS-PNVCL.

Drug-loaded NPs (DOX/ICG@Bio-CS-PNVCL NPs) were prepared by self-assembly. DOX· HCl (5 mg) and ICG (5 mg) were dissolved in a drop of DMSO.

Bio-CS-PNVCL (30 mg) was dissolved in 30 mL PBS and the two solutions combined. The mixture was stirred at 1000 rpm for 24 hours and then centrifuged at 11,000 rpm for 30 minutes to remove unloaded drug. Finally, drug-loaded NPs were dialyzed (MWCO 3500 Da) to remove any adsorbed drug. DOX@Bio-CS-PNVCL NPs were prepared in a similar way, but without inclusion of ICG in the solutions, and DOX@CS-PNVCL systems generated via the same route but with CS-PNVCL in place of Bio-CS-PNVCL.

2.3 Characterization

^{1}H and ^{13}C nuclear magnetic resonance (NMR) spectroscopy was performed with a DRX 400 spectrometer (Bruker). A Nicolet Nexus 670 spectrometer (Thermo Fisher) was used to collected Fourier transform infrared (FT-IR) spectra. The morphologies of the NPs were studied with a JEOL JEM 1200EX transmission electron microscope (TEM) and a FEI Nova Nano scanning electron microscope (SEM). A UV-3600 spectrophotometer (Shimadzu) was used to measure UV-vis spectra. Particle size was examined on a BI-200SM instrument (Brookhaven Instruments) through dynamic light scattering (DLS).

2.4 Encapsulation efficiency and drug loading

The encapsulation efficiency (EE) and drug loading (DL) of DOX and ICG in the NPs were calculated by UV-Vis measurements. Firstly, the absorbance of PBS solutions with different concentrations of DOX and ICG was measured to construct a standard curve for each. The supernatant obtained after centrifuging the drug-loaded NPs was then assayed and the concentrations of DOX and ICG were determined via absorbance at 481 nm (DOX) and 780 nm (ICG) . Finally, the EE and DL were calculated by the following formulae:

$$EE=(D_1-D_2)/D_1\times100\% \quad (1)$$

$$DL=(D_1-D_2)/m_t\times100\% \quad (2)$$

D_1 represents the total mass of DOX or ICG added, D_2 the mass of free DOX or ICG in the supernatant, and m_t the total mass of nanoparticles obtained.

2.5 Photothermal effects

To investigate the photothermal properties of the DOX/ICG@Bio-CS-PNVCL

NPs, the temperature change profiles of NP suspensions prepared at different concentrations were measured with varied laser power densities. Thermal images of the suspensions were also recorded using a thermal infrared imaging camera (FLIR A300, Shanghai Spectrum Electronic Technology Co., Ltd.). Photothermal stability was explored over five repeated heating and cooling cycles. The photothermal efficiency was calculated based on heating-cooling curves and the following equation [47, 48]:

$$\eta = h\,S(T_{Max} - T_{Sur}) - Qs / I(1-10^{-A}) \quad (3)$$

where η is the photothermal conversion efficiency, h and S are the heat transfer coefficient and surface area, T_{Max} and T_{Sur} are the equilibrium temperature and ambient temperature, Qs is the heat absorbed by quartz cell, I represents the power density of the laser and A the absorbance of the material at 808 nm.

2.6 Phase transition and drug release

In order to explore the phase transitions of Bio-CS-PNVCL at different temperatures, the material was dispersed in ultrapure water by sonication. The temperature of the solution (0.5 mg/mL) was increased slowly, and the absorbance recorded.

Drug release from DOX/ICG@Bio-CS-PNVCL under different conditions was also investigated. DOX/ICG@Bio-CS-PNVCL NPs (8 mg) were dispersed in PBS (pH 7.4 or 5.0; 8 mL). 2 mL of this suspension was loaded into a dialysis bag (MWCO: 3500 Da), and then placed in 30 mL of PBS solution. Experiments were performed at pH=7.4 and pH=5.0 in a shaker (100 rpm) at 37 ^{o}C. Samples (1 mL) were taken at specific times and the same volume of pre-warmed PBS solution (1 mL) was added to maintain a constant volume. In experiments with NIR irradiation, 2 h into the drug release experiment the NP suspensions were irradiated (808 nm, 1.0 W/cm^2) for five minutes when the drugs were released for two hours. UV-vis spectra were obtained on all the release aliquots and used to determine cumulative release.

2.7 *In vitro* cellular uptake

Confocal microscopy was carried out to explore the targeting ability of biotin. 4T1 and L929 cells were placed in culture dishes with 1×10^5 cells per dish (in 2 mL of

DMEM containing 10% FBS and 1% penicillin-streptomycin). The cells were incubated overnight (5% CO_2, 37 °C), and then 200 μL of the medium was removed and replaced with 200 μL of solutions or suspensions of free DOX, DOX@CS-PNVCL and DOX@Bio-CS-PNVCL in PBS. The final concentration of DOX in each dish was 0.5 μg/mL. A negative group comprised untreated cells. Four hours later, the medium was discarded and the cells were washed with PBS three times. Glutaraldehyde solution (5%, 1 mL) was added to each dish to fix the cells, and the culture dishes allowed to stand for 30 min at room temperature. Subsequently, DAPI solution (0.5 mL) was added to stain cell nuclei, and the dishes incubated for three minutes at room temperature. Finally, the cells were washed with PBS three times and observed by confocal laser scanning microscopy (FV1000, Olympus).

2.8 *In vitro* cytotoxicity

In order to determine the toxicity of the various materials to tumor cells, MTT experiments were performed. 4T1 cells were cultured in a 96-well plate (1×10^4 cells per well, 200 μL). They were incubated (5% CO_2, 37 °C) with DMEM medium containing 10% v/v FBS and 1% penicillin-streptomycin. After 24 hours, 20 μL solutions or suspensions of free DOX, Bio-CS-PNVCL, DOX@Bio-CS-PNVCL, or DOX/ICG@Bio-CS-PNVCL were added to replace 20 μL of DMEM in each well. Five solutions of each material were prepared in PBS, to give final concentrations of DOX of 0.01, 0.1, 1, 5 and 10 μg/mL. The concentration of Bio-CS-PNVCL used was equal to the concentration of Bio-CS-PNVCL in DOX-ICG@Bio-CS-PNVCL. Twenty independent experiments were performed with three replicate wells per condition in each experiment. In addition, cells treated with PBS (20 μL) comprised a negative control. After 24 hours, the medium was removed and cells washed with PBS three times. Then, MTT solution (100 μL) was added to each well and the plate incubated in the dark for 4 hours. DMSO (200 μL) was added and cells were incubated for 15 minutes more. Finally, the absorbance was read on microplate reader (Bio-Tek). The blank comprised a mixture of MTT solution and DMSO. Cell viability was calculated as:

$$\text{Cell viability} = (OD_{experiment}-OD_{blank}) / (OD_{control}-OD_{blank}) \times 100\% \quad (4)$$

The live-dead double staining assay and flow cytometry were also performed. The former was conducted by incubating 4T1 cells in a 6-well plate (1×10^5 cells per well, 2 mL of DMEM) for 24 hours (5% CO_2, 37 °C). The Calcein-AM/PI mixed solution was prepared according to the manufacturer instructions. Solutions or suspensions of the various formulations (200 μL) were added to the wells. The treatment groups comprised: PBS, free DOX, free ICG, Bio-CS-PNVCL, DOX@Bio-CS-PNVCL, DOX/ICG@Bio-CS-PNVCL. The final concentration of DOX was 0.5 μg/mL, and there were six independent experiments, each with an additional replicate well. The cells were incubated for 12 hours (5% CO_2, 37 °C), after which the medium was removed and the cells washed with PBS three times. Calcein-AM/PI staining solution (0.5 mL) was added to each well and the plates incubated in the dark for 45 min. Finally, the cells were washed and observed under an inverted fluorescence microscope (TE-2000 U, Olympus).

For flow cytometry, 4T1 cells were charged into a 6-well plate, incubated and treated with the various formulations as for the live-dead assay. Then, trypsin solution (0.25%, 0.5 mL) was added to digest the cells. Fresh medium (0.5 mL) was added to terminate digestion after three minutes. Subsequently, the cells were centrifuged at 1000 rpm for 3 min and washed twice with PBS. Finally, PBS (0.5 mL) was added to resuspend the cells, followed by Annexin V-FITC (5 μL) and PI (5 μL). The cells were incubated in the dark for 15 min and apoptosis quantified with flow cytometry (Becton Dickinson, Franklin Lakes, NJ).

2.9 *In vivo* anticancer efficacy

Female nude mice aged 4-6 weeks were used for these experiments. 4T1 cells (1×10^7 cells in 100 μL of DMEM) were injected subcutaneously into the right flank. When the tumor volume reached 100 mm^3 ($V=length\times width^2 / 2$), mice were randomly divided into 5 groups (4 mice/group) and treated with: PBS, free DOX, free ICG, DOX@Bio-CS-PNVCL and DOX-ICG@Bio-CS-PNVCL. Treatment was administrated via the tail vein, to give corresponding dosages of DOX and ICG of 5 and 7.5 mg/kg respectively. Nude mice in groups of free ICG and DOX/ICG@Bio-CS-PNVCL were irradiated with an NIR laser (1.0 W/cm^{-1}) for 5

min at 24 h after injection.

2.10 *In vivo* thermal imaging

4T1 tumor-bearing nude mice were injected with 100 μL of PBS, free ICG and DOX/ICG@Bio-CS-PNVCL via the tail vein to give an ICG dose of 5 mg/kg. Twenty-four hours after injection, nude mice were exposed to an NIR laser (808 nm, 1.0 W/cm^2) for 5 minutes, and *in vivo* real-time images were recorded with a thermal imaging camera (FLIR A300, Shanghai Spectrum Electronic Technology Co., Ltd.).

2.11 Histological analyses

After 14 days of treatment, mice were sacrificed and the heart, liver, spleen, lung, kidney and tumor tissues were excised. The tissues were then fixed with 4% formalin and embedded in paraffin, before being cut into fine slices for histological examination. Hematoxylin and eosin (H&E) and terminal deoxynucleotidyl transferase-mediated dUTP nick-end labeling (TUNEL) assays were used to analyse cell apoptosis, while Ki-67 staining was conducted to measure cell proliferation.

3 Results and discussion

3.1 Characterization of DOX-ICG@Bio-CS-PNVCL

The successful preparation of Bio-CS-PNVCL was verified by FT-IR and NMR spectra. FT-IR data (Figure 1a) reveal characteristic peaks from the primary alcohol and secondary alcohol of CS at 1022 cm^{-1} and 1064 cm^{-1}, respectively. The C=C and C-H functional groups of NVCL result in bands at 1653 cm^{-1} and 2931 cm^{-1}, respectively. The -$CONH_2$ and -COOH groups in biotin give peaks at 1637 cm^{-1} and 1684 cm^{-1}. In the spectrum of Bio-CS-PNVCL, the CS alcohol peaks are clearly visible. The biotin peak at 1634 cm^{-1} (-$CONH_2$) is still present, but the peak at 1684 cm^{-1} disappears, suggesting that biotin was grafted to CS via an amide bond. The C-H group in NVCL can be seen at 2919 cm^{-1} in the spectrum of Bio-CS-PNVCL, but the C=C functional group band has disappeared, indicating that NVCL was successfully polymerized onto the CS.

NMR spectra further proved the successful modification of CS. Compared to the spectrum of CS (Figure 1c), the peak intensity at 1.98 ppm is significantly enhanced

in the ^{1}H NMR spectrum of N-CS (Figure S1), which is attributed to the methyl group present in the acetyl modification. The ^{1}H NMR spectrum of CS-RAFT (Figure 1c) includes methyl and methylene peaks between 0.80-2.00 ppm from DDACT (see Figure S2 for DDACT spectrum), a characteristic O**H** peak resonance around 5.58 ppm from CS, and an imine proton at ca. 7.41 ppm, demonstrating that DDACT was grafted onto CS. The ^{13}C NMR spectrum (Figure 1b) displays resonances at 169.5 ppm, 157.1 ppm, and 153.4 ppm. These correspond to **C**=S, amide, and ester groups, respectively. The formation of the CS-RAFT species is thus clearly evidenced.

The ^{1}H NMR spectrum of Bio-CS-PNVCL is given in Figure 1c. Peaks at ca. 7.22 ppm are clearly visible in the NVCL spectrum (Figure S3), corresponding to the C=C**H** proton. These have disappeared for Bio-CS-PNVCL, confirming the polymerization of NVCL. Comparing this with the spectra of NVCL and biotin (Figure S3 and S4), the peaks at 8.13 ppm and 7.84 ppm in can be attributed to the amide groups of biotin and chitosan, respectively. The signal at 5.32 ppm is attributed to the O**H** proton of chitosan. Peaks at 1.49-2.09 ppm correspond to the methylene groups of PNVCL, and that at 0.85 ppm to the methyl of the RAFT agent. The above results demonstrate the successful grafting of CS. Based on the ^{1}H NMR spectrum of DOX/ICG@Bio-CS-PNVCL (Figure 1c), the degree of substitution of RAFT on chitosan was calculated to be 1. The UV-Vis spectrum of DOX/ICG@Bio-CS-PNVCL NPs (Figure S5) showed the characteristic peaks of DOX and ICG at 481 nm and 780 nm respectively, demonstrating the successful loading of DOX and ICG.

The hydrodynamic diameter of DOX-ICG@Bio-CS-PNVCL NPs was determined by DLS and found to be 115 ± 6 nm (Figure 1d). This is much smaller than previously reported chitosan-based nanoparticles [24], and suitable for passive targeting of tumor cells via the EPR effect. The morphology of the DOX-ICG@Bio-CS-PNVCL NPs was characterized by TEM (Figure 1e) and SEM (Figure 1f). The NPs are spherical. The particle size in TEM is smaller than the hydrodynamic diameter measured by DLS, which may be the result of drying and

dehydration during sample preparation. The TEM image indicates the presence of some core/shell structure, consistent with segregation of the hydrophobic segments of the Bio-CS-PNVCL polymer into the core, away from the aqueous environment used for self assembly. The drug loading was found to be 9.5 ± 1.5% and 12.3 ± 0.7% for DOX and ICG respectively. This is similar to other reported chitosan-based drug-loaded NPs [25]. The encapsulation efficiencies were 73.7 ± 12.0% (DOX) and 92.7 ± 9.5% (ICG).

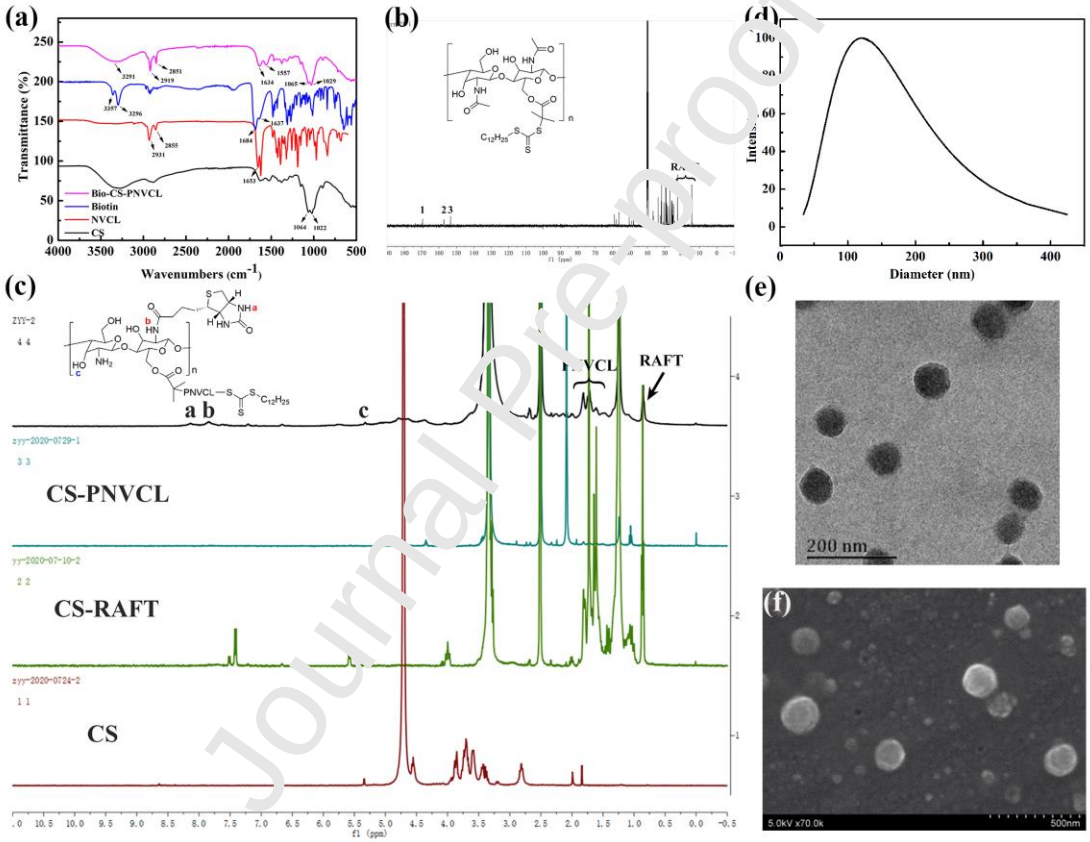

Figure 1 (a) FT-IR spectra of CS, NVCL, Biotin and Bio-CS-PNVCL; (b) ^{13}C NMR spectrum of CS-RAFT (resonances 1 (169.5 ppm), 2 (157.1 ppm), and 3 (153.4 ppm) correspond to **C**=S, amide, and ester groups); (c) ^{1}H NMR spectra of CS, CS-RAFT, CS-PNVCL and Bio-CS-PNVCL (resonances a (8.13 ppm), b (7.84 ppm) and c (5.32 ppm) are attributed to the amide groups of biotin and chitosan and to the chitosan O**H** proton); (d) DLS data on DOX/ICG@Bio-CS-PNVCL NPs; (e) TEM and (f) SEM images of DOX/ICG@Bio-CS-PNVCL NPs.

3.2 Photothermal effects

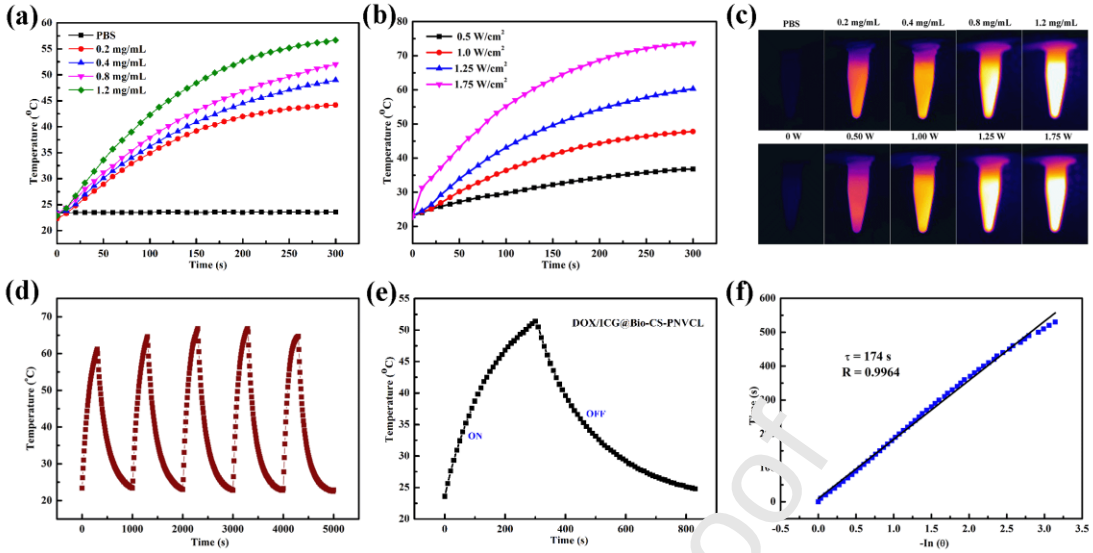

Figure 2 Photothermal properties of DOX/ICG@Bio-CS-PNVCL. Temperature variation curves of suspensions (a) at different concentrations under NIR irradiation at 808 nm / 1.0 W/cm^2 and (b) 0.8 mg/mL with varied NIR laser power densities. (c) Photothermal images at top: different NP concentrations (1.0 W/cm^2) and bottom: varied NIR laser power densities (0.8 mg/mL). (d) Temperature profile over five heating-cooling cycles (1.25 W/cm^2). (e) Heating-cooling curve with 5 minutes of NIR laser irradiation (0.8 mg/mL, 1.0 W/cm^2); (f) Linear regression of cooling stage.

Upon NIR irradiation, the temperature of the DOX/ICG@Bio-CS-PNVCL NPs suspension increased continuously, with a greater NP concentration resulting in a greater temperature elevation (Figure 2a). At a fixed concentration, the temperature rise increases with elevated laser power density (Figure 2b). Figure 2c shows photothermal images of DOX/ICG@Bio-CS-PNVCL after laser irradiation, indicating that these temperature changes can be clearly observed visually. This could aid the development of targeted drug delivery systems and/or theranostics. The particle size of the NPs was found to increase to 425 nm after irradiation. This is attributed to the PTT properties of ICG, which causes thermal expansion and also potentially the aggregation of particles.

To explore the robustness of the NP platform, five heating and cooling cycles

were performed on the same suspension (Figure 2d). The maximum temperature is largely unchanged across these cycles, confirming that DOX/ICG@Bio-CS-PNVCL possesses good photothermal stability. This is due to the loading of ICG in the nanoparticles, which protects it from the photobleaching typically seen with ICG [49, 50]. The photothermal conversion efficiency (PTCE) was calculated from heating-cooling curves (Figure 2e) and linear regression (Figure 2f) of the cooling stage. The PTCE is 29.3%, similar to previously reported ICG-loaded nanoplatforms [51].

3.3 Phase transition and drug release

The phase transition of Bio-CS-PNVCL was analysed by measuring absorbance at 500 nm as a function of temperature (Figure 3a). The absorbance can be seen to reduce as the temperature increased. This phenomenon is due to the phase transition of the PNVCL. At room temperature, Bio-CS-PNVCL is dispersed in water by hydrogen bonding, forming an opaque suspension with high absorbance. When the temperature rose above the PNVCL lower critical solution temperature (LCST), the hydrogen bonds were broken and Bio-CS-PNVCL was precipitated out of solution and deposited on the bottom. This results in the supernatant becoming transparent and thus causing a reduction in absorbance. This phase transition behavior is contrary to the usual LCST behavior [52, 53], where the polymer dissolves at temperature below the LCST, and phase separation occurs in the polymer solution when the temperature is above the LCST [54], and is believed to arise because the nanoparticles have low-density structures in which there is water ingress into the core, and thus interactions between PNVCL and water molecules.

Drug release experiments (Figure 3b) were carried out to investigate the influence of pH value and NIR irradiation. The extent of DOX release at pH=5.0 is notably higher than at pH=7.4. This is because the solubility of chitosan and DOX is enhanced in acidic conditions, which promotes release of the DOX cargo. The application of NIR irradiation increases the extent of DOX release at a given pH: ICG generates heat under NIR exposure, promoting a hydrophilic-hydrophobic phase transition in the PNVCL component of the NPs. As a result of this, the NPs shrink to a

smaller size squeezing the DOX out of the core.

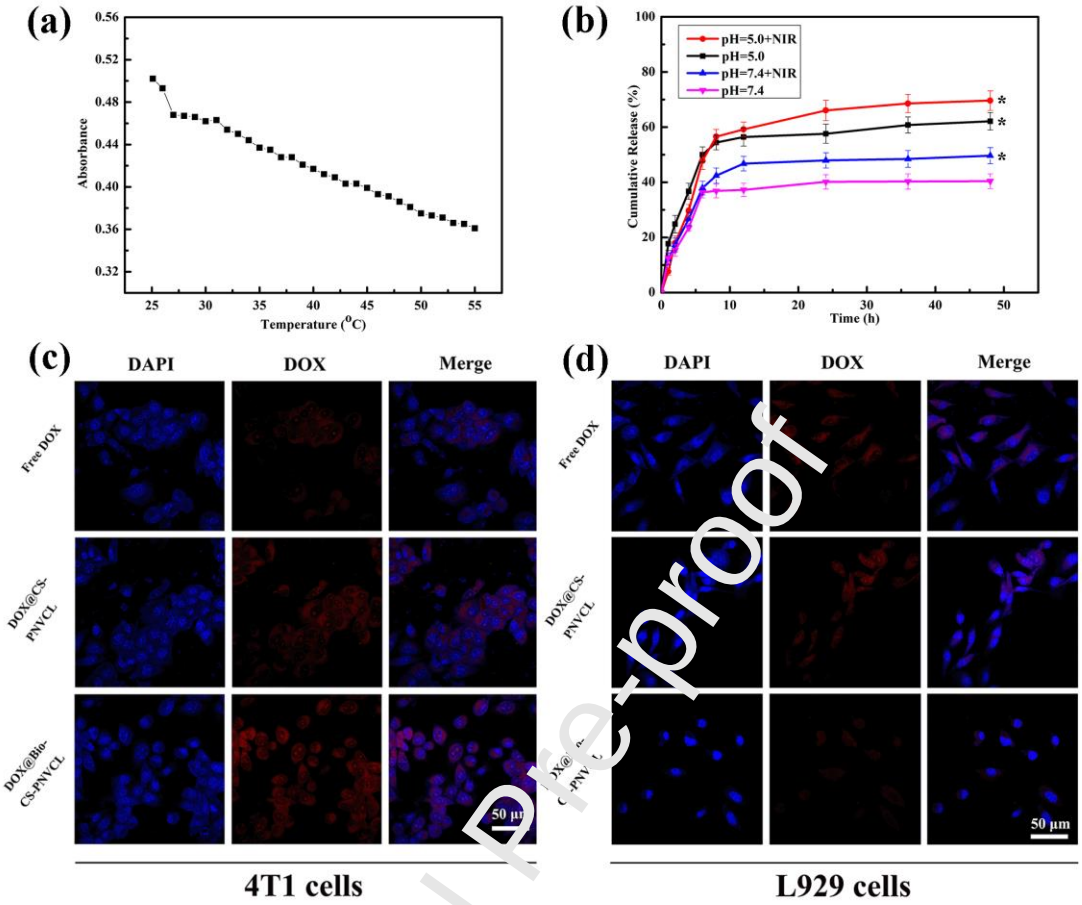

Figure 3 (a) The absorbance at 808 nm of Bio-CS-PNVCL suspensions as a function of temperature; (b) release of DOX from the NPs under different conditions (*$p < 0.05$, compared to pH=7.4); confocal microscopy images of (c) 4T1 cells and (d) L929 cells treated with free DOX, DOX@CS-PNVCL, or DOX@Bio-CS-PNVCL for 4 hours.

3.4 *In vitro* cellular uptake

The cellular uptake efficiency was explored by CLSM (Figure 3c and 3d). Minimal red fluorescence (arising from DOX) is seen when cells are incubated with DOX alone. This is slightly increased when DOX@CS-PNVCL NPs are used. When incubated with DOX@Bio-CS-PNVCL for 4 hours, 4T1 cells showed notably enhanced red flourescence, while L929 cells displayed weaker signals, implying that NPs are more effectively taken up by cancerous 4T1 cells than healthy L929 cells. 4T1 cells exposed to DOX@Bio-CS-PNVCL depicted a greatest extent of red fluorescence, which was attributed to the biotin endowing the NPs with the ability to

actively target cancer cells.

3.5 *In vitro* cytotoxicity

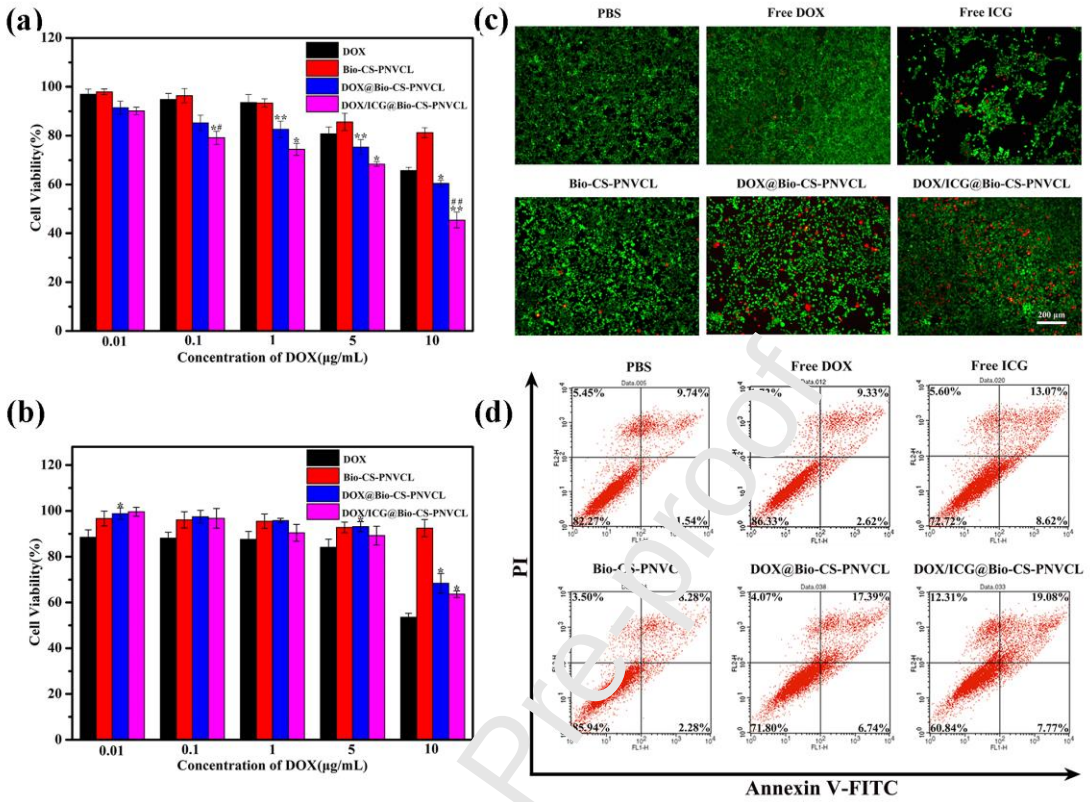

Figure 4 Cell viability of (a) 4T1 cells and (b) L929 cells incubated with DOX, Bio-CS-PNVCL, DOX@Bio-CS-PNVCL and DOX-ICG@Bio-CS-PNVCL (*p<0.05, **p<0.01, compared to DOX; #p<0.05, ##p<0.01, compared to DOX@Bio-CS-PNVCL); (c) fluorescence images of 4T1 cells stained with Calcein-AM/PI after different treatments; (d) flow cytometry analysis of 4T1 cells after various treatments. Early apoptotic, late apoptotic and necrotic cells lie in the lower right, upper right and upper left quadrant, respectively.

The effect of the formulations on the viability of 4T1 (Figure 4a) and L929 (Figure 4b) cells was assessed by MTT assays. The toxicity of DOX/ICG@Bio-CS-PNVCL on 4T1 cells was concentration-dependent. When the corresponding concentration of DOX reached 10 μg/mL, the cell viability in the DOX/ICG@Bio-CS-PNVCL group was ca. 50%. Free DOX and DOX @Bio-CS-PNVCL are notably less cytotoxic, while even high concentrations of

Bio-CS-PNVCL led to minimal loss of viability. This shows the carrier to be non-toxic, and that the use of the biotin conjugated NPs can enhance cytotoxic effects over the free API.

With L929, the NPs do not result in any toxicity when the concentration of DOX is below 5 μg/mL. Free DOX does result in some cell death (ca. 10 – 20%). The DOX/ICG@Bio-CS-PNVCL NPs did display some toxicity to L929 cells at the highest concentration of 10 μg/mL. However, in comparison to free DOX, they showed markedly attenuated cell toxicity, indicating that the nanocomposites possess targeted delivery properties. The Bio-CS-PNVCL carrier is not toxic even at the highest concentration of 10 μg/mL.

Calcein-AM/PI double staining results are depicted in Figure 4c. The number of red (apoptotic) cells is highest in the DOX-ICG@Bio-CS-PNVCL group, implying this gives the greater amount of cell death. Some cell death is noted with DOX@Bio-CS-PNVCL, but markedly less. Furthermore, the Bio-CS-PNVCL group displayed very little red fluorescence, which confirms the MTT results and demonstrates that the nanocarrier is non-toxic to cells. Free DOX results in less toxicity than the DOX-ICG@Bio-CS-PNVCL treatment, likely due to the lack of targeting of free DOX. Less DOX was taken up by cells, resulting in less cytotoxicity. However, the free ICG group did demonstrate some degree of toxicity, because under NIR irradiation ICG can generate heat and thus promote cell apoptosis.

Flow cytometric analysis (Figure 4d) was conducted to confirm the MTT and live/dead results. The cell apoptosis rates of the free DOX and PBS groups were almost equal, indicating that free DOX lacked targeting and showed little toxicity to cells. The apoptosis rate (27.28%) of the free ICG group was clearly higher, which is the result of photothermal therapy. The apoptosis rate of the Bio-CS-PNVCL group was 14.06%, also similar to the PBS group, again indicating that the nanocarrier was not toxic to cells and consistent with the live-dead staining results. The DOX@Bio-CS-PNVCL group had enhanced cytotoxicity (28.20%), which was due to the loading of DOX in the nanocarrier, leading to both passive and active targeting and drug release in the cytosol. As previously, the DOX-ICG@Bio-CS-PNVCL group

showed the highest level (39.2%) of early/late apoptosis and necrosis, as a result of preferential uptake and synergistic photothermal and chemotherapy.

3.6 *In vivo* therapeutic efficacy

Therapeutic effects *in vivo* were evaluated in 4T1 tumor-bearing mice. All mice in the free ICG and DOX/ICG@Bio-CS-PNVCL groups received NIR irradiation (808 nm) during treatment. Tumor photos and tumor masses obtained after the treatment period (Figure 5a) showed that DOX/ICG@Bio-CS-PNVCL effectively inhibited tumor growth, and that the combination of photothermal and chemotherapy significantly improved the treatment efficacy. The relative tumor volume change curves (Figure 5b) reveal that the tumor volume in the control group increased rapidly over time, while the tumor volume of the DOX/ICG@Bio-CS-PNVCL group displayed no observable changes. Free DOX and free ICG were able to cause some suppression of the tumor growth, while DOX/ICG@CS-PNVCL performed better. The enhanced efficacy of DOX/ICG@Bio-CS-PNVCL is clearly evidenced from these data.

Plots of body weight vs time (Figure 5c) show a general decline for the free DOX group, due to the fact that DOX is non-targeted and causes off-target side effects as reported previously [55, 56]. The body weights in the other groups remained largely stable, indicating good biocompatibility.

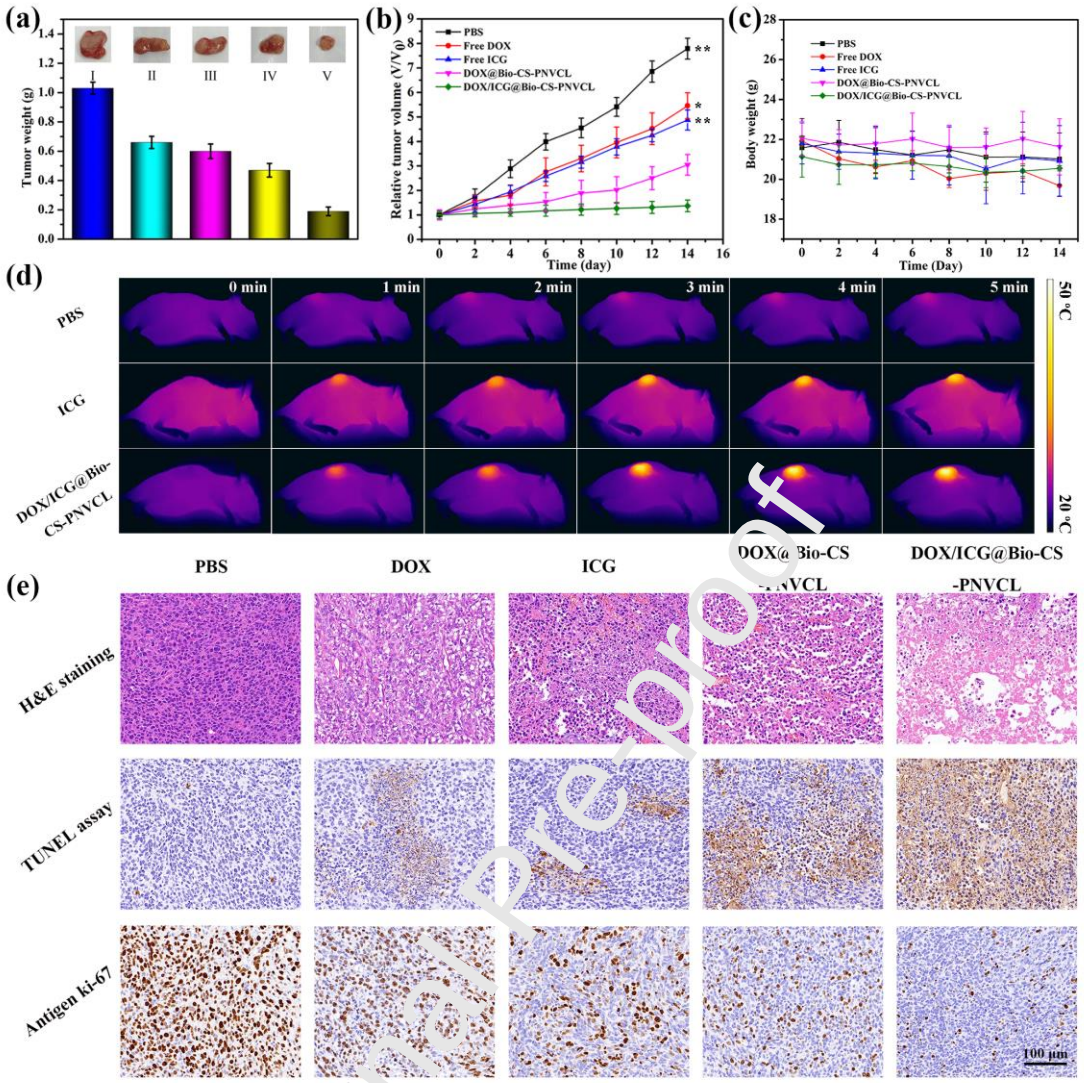

Figure 5 (a) Photos and masses of tumors excised from mice in the different treatment groups at the end of the in vivo experiment (Ⅰ: PBS, Ⅱ: Free DOX, Ⅲ: Free ICG, Ⅳ: DOX@Bio-CS-PNVCL, Ⅴ:DOX/ICG@Bio-CS-PNVCL); (b) Relative tumor volume (*$p < 0.05$, **$p < 0.01$, compared to DOX/ICG@Bio-CS-PNVCL) and (c) body weight recorded during the treatment processes; (d) thermal images in groups of mice treated with PBS, ICG or DOX/ICG@Bio-CS-PNVCL after 5 minutes of NIR irradiation; (e) H&E, TUNEL, and Antigen ki-67 staining of tumor sections from the different treatment groups (scale bars: 100 μm).

3.7 *In vivo* thermal imaging

In a separate experiment, three tumor-bearing mice were treated with PBS, ICG or DOX/ICG@Bio-CS-PNVCL respectively and exposed to NIR laser (1.0 W/cm^{-1}, 5

min) at 24h after injection. Images (Figure 5d) were recorded with a thermal camera. In the control group, the temperature at the tumor site displayed only small changes ($\Delta T = 3.2\ ^{o}C$). In contrast, the temperature of the tumor in the free ICG group rose to 45.3 ^{o}C, indicating the excellent photothermal conversion efficiency of ICG. The tumor temperature in the DOX/ICG@Bio-CS-PNVCL group increased still further, to 49.4 ^{o}C. This is higher than that in the free ICG group, indicating that the EPR effect and targeting ability of biotin allowed the accumulation of NPs at tumor site, increasing the local ICG concentration in the tumor.

3.8 Histological analysis

Histological analyses obtained on tumor sections are reported in Figure 5e. The DOX/ICG@Bio-CS-PNVCL treatment group revealed the most distinct cell apoptosis in H&E staining, while the control group showed no cell damage. The DOX, ICG and DOX/ICG@CS-PNVCL showed a limited amount of damage. In TUNEL staining, a similar trend could be seen. Tumor sections from DOX/ICG@Bio-CS-PNVCL-treated mice displayed the largest quantity of apoptotic cells (brown-stained), while notably smaller numbers of apoptotic cells can be seen with the other treatment groups. Immunohistochemical staining was conducted to analyse the cell proliferation in the tumor. Antigen Ki67 staining revealed that DOX/ICG@Bio-CS-PNVCL group had the fewest proliferating cells (brown) and the largest area of cell damage (blue), showing the NPs are better able to kill cells and prevent their proliferation in comparison with other groups. All these results comprehensively demonstrate the excellent anti-cancer therapeutic effects of DOX/ICG@Bio-CS-PNVCL NPs.

H&E staining was also performed on the major organs after treatment (Figure 6) The free DOX treatment resulted in some off-target effects, which can be seen in terms of vacuolar degeneration in the spleen and kidney. However, no obvious damage can be seen after the other treatments, suggesting DOX/ICG@Bio-CS-PNVCL NPs and the other materials have negligible systemic toxicity.

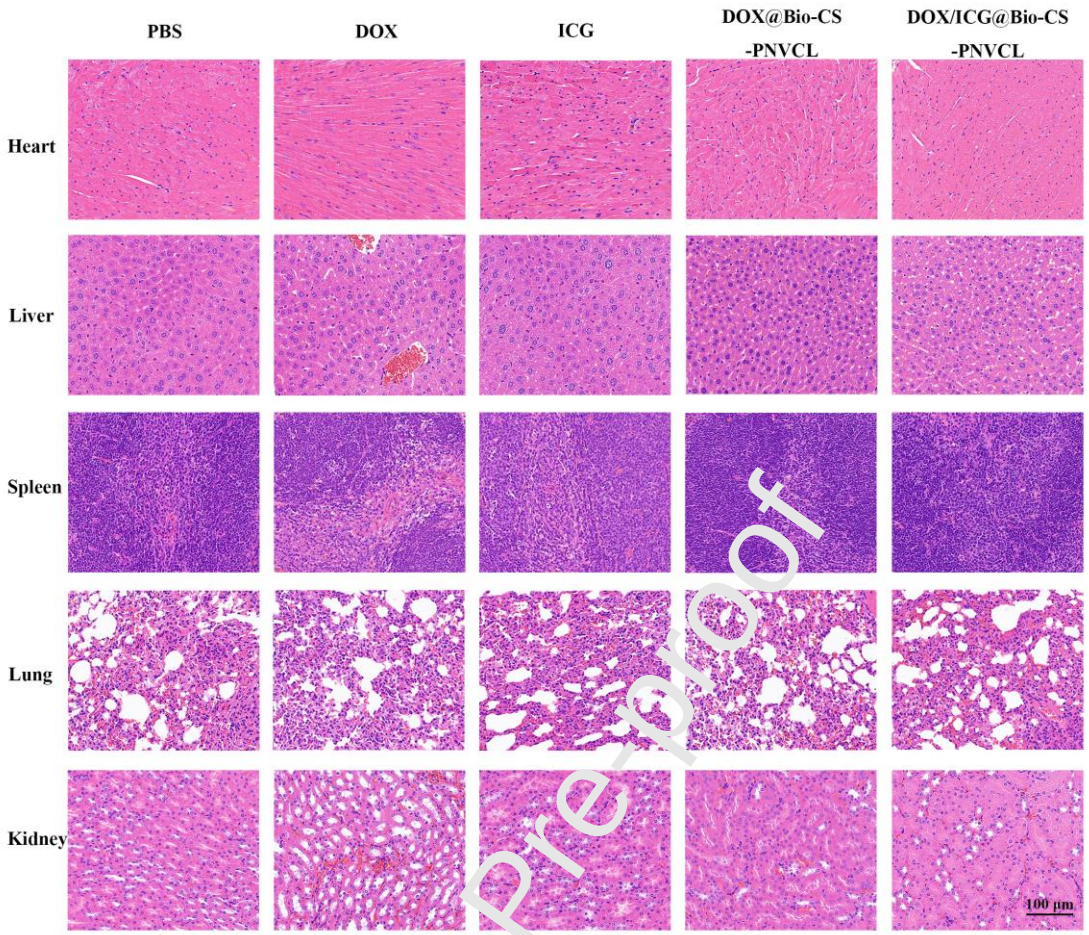

Figure 6 H&E staining of heart, liver, spleen, lung and kidney sections after treatment with PBS, DOX, ICG, DOX@Bio-CS-PNVCL, DOX/ICG@Bio-CS-PNVCL (scale bars: 100 μm).

4. Conclusions

In this work, chitosan-based thermosensitive DOX/ICG@Bio-CS-PNVCL NPs were fabricated to co-deliver the photothermal agent ICG and chemotherapeutic drug DOX. These materials are found to have particle sizes of 115±6 nm, suitable for uptake and retention in tumors via the EPR effect, and have potent photothermal properties. The presence of the targeting agent biotin in the formulation was observed to aid NP uptake into cancer cells. Drug release from the NPs is triggered by both NIR exposure and reduced pH conditions. The NPs were further able to cause effective cancer cell death both in vitro and in vivo, with tumor growth notably suppressed in a xenograft mouse model of breast cancer. Tissue sections showed that the NPs were

able to reduce the off-target damage to healthy tissues caused by DOX, compared with the free DOX group, but promoted cell death and inhibited cell proliferation in the tumor. DOX/ICG@Bio-CS-PNVCL NPs thus comprise an intelligent drug delivery platform with potential in combined photothermal and chemotherapy of breast cancer.

CRediT authorship contribution statement

Yanyan Zhang: Conceptualization; Data curation; Formal analysis; Investigation; Methodology; Software; Validation; Visualization; Writing - original draft. **Gareth R. Williams:** Writing - review & editing. **Jiadong Lou:** Validation; Visualization. **Wanting Li:** Validation; Visualization. **Cuiwei Bai:** Validation; Visualization. **Tong Wang:** Software; Validation; Visualization. **Shiwei Niu:** Conceptualization; Formal analysis; Funding acquisition; **Chun Feng:** Funding acquisition; Project administration; Resources; Supervision; Writing - review & editing. **Li-Min Zhu:** Conceptualization; Formal analysis; Funding acquisition; Methodology; Project administration; Resources; Supervision; Writing - review & editing.

Declaration of competing interest

All authors declare that no competing interests exist.

Acknowledgements

This investigation was financially supported by grants 22520710400, 21WZ2501300 and 20DZ2254900 from the Science and Technology Commission of Shanghai Municipality, the Biomedical Textile Materials “111 Project” of the Ministry of Education of China (No. B07024) and Yunnan Provincial Department of Science and Technology-Kunming Medical University Joint Project on Applied Basic Research (202201AY070001-029 / 2019FE001(-007)).

References

[1] K. Guo, Y. Liu, L. Tang, Q.T.H. Shubhra, Homotypic biomimetic coating synergizes chemo-photothermal combination therapy to treat breast cancer overcoming drug resistance, Chemical Engineering Journal 428 (2022) 131120.

[2] B. Li, T. Tan, W. Chu, Y. Zhang, Y. Ye, S. Wang, Y. Qin, J. Tang, X. Cao, Co-delivery of paclitaxel (PTX) and docosahexaenoic acid (DHA) by targeting lipid nanoemulsions for cancer therapy, Drug Deliv 29(1) (2022) 75-88.

[3] M. Rizwanullah, M.Z. Ahmad, M.M. Ghoneim, S. Alshehri, S.S. Imam, S. Md, N.A. Alhakamy, K. Jain, J. Ahmad, Receptor-Mediated Targeted Delivery of Surface-Modified Nanomedicine in Breast Cancer: Recent Update and Challenges, Pharmaceutics 13(12) (2021) 2039.

[4] Y.C. Zhang, P.Y. Zeng, Z.Q. Ma, Z.Y. Xu, Z.K. Wang, B. Guo, F. Yang, Z.T. Li, A pH-responsive complex based on supramolecular organic framework for drug-resistant breast cancer therapy, Drug Deliv 29(1) (2022) 128-137.

[5] Y. Guo, S. Liu, F. Luo, D. Tang, T. Yang, X. Yang, Y. Xie, A Nanosized Codelivery System Based on Intracellular Stimuli-Triggered Dual-Drug Release for Multilevel Chemotherapy Amplification in Drug-Resistant Breast Cancer, Pharmaceutics 14(2) (2022) 422.

[6] Y. Yuan, J. Liu, X. Xu, X. Liu, Y. Cheng, C. Zhou, M. Li, L. Shi, Y. Deng, H. Liu, G. Wang, L. Wang, Z. Wang, Tumor-targeting pH/redox dual-responsive nanosystem epigenetically reverses cancer drug resistance by co-delivering doxorubicin and GCN5 siRNA, Acta Biomater 135 (2021) 556-566.

[7] L. Tang, A. Zhang, Y. Mei, Q. Xiao, X. Xu, W. Wang, NIR Light-Triggered Chemo-Phototherapy by ICG Functionalized MWNTs for Synergistic Tumor-Targeted Delivery, Pharmaceutics 13(12) (2021) 2145.

[8] W. Feng, W. Shi, S. Liu, H. Liu, Y. Liu, P. Ge, H. Zhang, Fe(III)-Shikonin

Supramolecular Nanomedicine for Combined Therapy of Tumor via Ferroptosis and Necroptosis, Adv Healthc Mater 11(2) (2022) e2101926.

[9] K. Li, C. Lin, M. Li, K. Xu, Y. He, Y. Mao, L. Lu, W. Geng, X. Li, Z. Luo, K. Cai, Multienzyme-like Reactivity Cooperatively Impairs Glutathione Peroxidase 4 and Ferroptosis Suppressor Protein 1 Pathways in Triple-Negative Breast Cancer for Sensitized Ferroptosis Therapy, ACS Nano 16(2) (2022) 2381-2398.

[10] R. Xie, S. Ruan, J. Liu, L. Qin, C. Yang, F. Tong, T. Lei, M. Shevtsov, H. Gao, Y. Qin, Furin-instructed aggregated gold nanoparticles for re-educating tumor associated macrophages and overcoming breast cancer chemoresistance, Biomaterials 275 (2021) 120891.

[11] S. Gou, N. Chen, X. Wu, M. Zu, S. Yi, B. Ying, F. Dai, B. Ke, B. Xiao, Multi-responsive nanotheranostics with enhanced tumor penetration and oxygen self-producing capacities for multimodal synergistic cancer therapy, Acta Pharm Sin B 12(1) (2022) 406-423.

[12] X. Xu, R. Zhang, X. Yang, Y. Lu, Z. Yang, M. Peng, Z. Ma, J. Jiao, L. Li, A Honeycomb-Like Bismuth/Manganese Oxide Nanoparticle with Mutual Reinforcement of Internal and External Response for Triple-Negative Breast Cancer Targeted Therapy, Adv Healthc Mater 10(18) (2021) e2100518.

[13] S. Peng, F. Xiao, M. Chen, H. Gao, Tumor-Microenvironment-Responsive Nanomedicine for Enhanced Cancer Immunotherapy, Adv Sci (Weinh) 9(1) (2022) e2103836.

[14] W. Wang, X. Zhang, Z. Li, D. Pan, H. Zhu, Z. Gu, J. Chen, H. Zhang, Q. Gong,

K. Luo, Dendronized hyaluronic acid-docetaxel conjugate as a stimuli-responsive nano-agent for breast cancer therapy, Carbohydr Polym 267 (2021) 118160.

[15] L. Fang, Z. Zhao, J. Wang, P. Xiao, X. Sun, Y. Ding, P. Zhang, D. Wang, Y. Li, Light-controllable charge-reversal nanoparticles with polyinosinic-polycytidylic acid for enhancing immunotherapy of triple negative breast cancer, Acta Pharm Sin B 12(1) (2022) 353-363.

[16] L. Yang, X. Hou, Y. Zhang, D. Wang, J. Liu, F. Huang, J. Liu, NIR-activated self-sensitized polymeric micelles for enhanced cancer chemo-photothermal therapy, J Control Release 339 (2021) 114-129.

[17] J. Flynn, E. Durack, M.N. Collins, S.P. Hudson, Tuning the strength and swelling of an injectable polysaccharide hydrogel and the subsequent release of a broad spectrum bacteriocin, nisin A, J Mater Chem B 8(18) (2020) 4029-4038.

[18] K. Valachova, K. Svik, C. Biro, M.N. Collins, R. Jurcik, L. Ondruska, L. Soltes, Impact of Ergothioneine, Hercynine, and Histidine on Oxidative Degradation of Hyaluronan and Wound Healing, Polymers (Basel) 13(1) (2020) 95.

[19] L. Jiang, Y. Wang, X. Wei, L. Yang, S. Liu, Y. Wang, Y. Xu, Z. Wang, C. Zhang, M. Zhang, Y. Zhang, F. Jin, X. Yin, Improvement in phenotype homeostasis of macrophages by chitosan nanoparticles and subsequent impacts on liver injury and tumor treatment, Carbohydr Polym 277 (2022) 118891.

[20] P. Song, N. Song, L. Li, M. Wu, Z. Lu, X. Zhao, Angiopep-2-Modified Carboxymethyl Chitosan-Based pH/Reduction Dual-Stimuli-Responsive Nanogels for Enhanced Targeting Glioblastoma, Biomacromolecules 22(7) (2021) 2921-2934.

[21] M. Fathi, P.S. Zangabad, A. Aghanejad, J. Barar, H. Erfan-Niya, Y. Omidi, Folate-conjugated thermosensitive O-maleoyl modified chitosan micellar nanoparticles for targeted delivery of erlotinib, Carbohydr Polym 172 (2017) 130-141.

[22] T.T.V. Phan, M.S. Moorthy, H.W. Kang, S.Y. Nam, Y.W. Lee, J. Oh, Coating Chitosan Thin Shells: A Facile Technique to Improve Dispersion Stability of Magnetoliposomes, J Nanosci Nanotechnol 18(1) (2018) 583-590.

[23] W. Wang, Q. Zhang, M. Zhang, X. Lv, Z. Li, M. Mohammadniaei, N. Zhou, Y. Sun, A novel biodegradable injectable chitosan hydrogel for overcoming postoperative trauma and combating multiple tumors, Carbohydr Polym 265 (2021) 118065.

[24] X. Zhang, S. Niu, G.R. Williams, J. Wu, X. Chen, H. Zheng, L.M. Zhu, Dual-responsive nanoparticles based on chitosan for enhanced breast cancer therapy, Carbohydr Polym 221 (2019) 84-93.

[25] X. Chen, S. Niu, D.H. Bremner, X. Zhang, H. Zhang, Y. Zhang, S. Li, L.M. Zhu, Co-delivery of doxorubicin and oleanolic acid by triple-sensitive nanocomposite based on chitosan for effective promoting tumor apoptosis, Carbohydr Polym 247 (2020) 116672.

[26] H. Kang, S. Hu, M.H. Cho, S.H. Hong, Y. Choi, H.S. Choi, Theranostic Nanosystems for Targeted Cancer Therapy, Nano Today 23 (2018) 59-72.

[27] S. Gai, G. Yang, P. Yang, F. He, J. Lin, D. Jin, B. Xing, Recent advances in functional nanomaterials for light–triggered cancer therapy, Nano Today 19 (2018) 146-187.

[28] X. He, Y. Hao, B. Chu, Y. Yang, A. Sun, K. Shi, C. Yang, K. Zhou, Y. Qu, H. Li, Z. Qian, Redox-activatable photothermal therapy and enzyme-mediated tumor starvation for synergistic cancer therapy, Nano Today 39 (2021) 101174.

[29] Z. Yang, L. Zhang, J. Wei, R. Li, Q. Xu, H. Hu, Z. Xu, J. Ren, C.Y. Wong, Tumor acidity-activatable photothermal/Fenton nanoagent for synergistic therapy, J Colloid Interface Sci 612 (2022) 355-366.

[30] Z. Yuan, B. Tao, Y. He, C. Mu, G. Liu, J. Zhang, Q. Liao, P. Liu, K. Cai, Remote eradication of biofilm on titanium implant via near-infrared light triggered photothermal/photodynamic therapy strategy, Biomaterials 223 (2019) 119479.

[31] H. Guo, L. Liu, Q. Hu, H. Dou, Monodisperse ZIF-8@dextran nanoparticles co-loaded with hydrophilic and hydrophobic functional cargos for combined near-infrared fluorescence imaging and photothermal therapy, Acta Biomater 137 (2022) 290-304.

[32] M. Li, X. Bian, X. Chen, N. Fan, H. Zou, Y. Bao, Y. Zhou, Multifunctional liposome for photoacoustic/ultrasound imaging-guided chemo/photothermal retinoblastoma therapy, Drug Deliv 29(1) (2022) 519-533.

[33] X. Sun, Y. Xu, Q. Guo, N. Wang, B. Wu, C. Zhu, W. Zhao, W. Qiang, M. Zheng, A Novel Nanoprobe for Targeted Imaging and Photothermal/Photodynamic Therapy of Lung Cancer, Langmuir 38(4) (2022) 1360-1367.

[34] Y. Chen, Y. Li, J. Liu, Q. Zhu, J. Ma, X. Zhu, Erythrocyte membrane bioengineered nanoprobes via indocyanine green-directed assembly for single NIR laser-induced efficient photodynamic/photothermal theranostics, J Control Release

335 (2021) 345-358.

[35] Q. Hu, K. Wang, L. Qiu, 6-Aminocaproic acid as a linker to improve near-infrared fluorescence imaging and photothermal cancer therapy of PEGylated indocyanine green, Colloids Surf B Biointerfaces 197 (2021) 111372.

[36] X. Li, Y. Pan, J. Zhou, G. Yi, C. He, Z. Zhao, Y. Zhang, Hyaluronic acid-modified manganese dioxide-enveloped hollow copper sulfide nanoparticles as a multifunctional system for the co-delivery of chemotherapeutic drugs and photosensitizers for efficient synergistic antitumor treatments, J Colloid Interface Sci 605 (2022) 296-310.

[37] B. Iyisan, J. Simon, Y. Avlasevich, S. Baluschev, V. Mailaender, K. Landfester, Antibody-Functionalized Carnauba Wax Nanoparticles to Target Breast Cancer Cells, ACS Appl Bio Mater 5(2) (2022) 622-629.

[38] R.Q. Yang, P.Y. Wang, K.L. Lou, Y.Y. Dang, H.N. Tian, Y. Li, Y.Y. Gao, W.H. Huang, Y.Q. Zhang, X.L. Liu, G.J. Zhang, Biodegradable Nanoprobe for NIR-II Fluorescence Image-Guided Surgery and Enhanced Breast Cancer Radiotherapy Efficacy, Adv Sci (Weinh) 9(12) (2022) e2104728.

[39] X. Zhang, B. Qin, M. Wang, J. Feng, C. Zhang, C. Zhu, S. He, H. Liu, Y. Wang, S.E. Averick, N.T.N. Vo, L. Huang, W. Liu, Z. Wang, Dual pH-Responsive and Tumor-Targeted Nanoparticle-Mediated Anti-Angiogenesis siRNA Delivery for Tumor Treatment, Int J Nanomedicine 17 (2022) 953-967.

[40] B.K. Kundu, Pragti, W.A. Carlton Ranjith, U. Shankar, R.R. Kannan, S.M. Mobin, A. Bandyopadhyay, S. Mukhopadhyay, Cancer-Targeted

Chitosan-Biotin-Conjugated Mesoporous Silica Nanoparticles as Carriers of Zinc Complexes to Achieve Enhanced Chemotherapy In Vitro and In Vivo, ACS Appl Bio Mater 5(1) (2022) 190-204.

[41] H. Shi, N. Liang, J. Liu, S. Li, X. Gong, P. Yan, S. Sun, AIE-active polymeric micelles based on modified chitosan for bioimaging-guided targeted delivery and controlled release of paclitaxel, Carbohydr Polym 269 (2021) 118327.

[42] H. Horo, M. Saha, H. Das, B. Mandal, L.M. Kundu, Synthesis of highly fluorescent, amine-functionalized carbon dots from biotin-modified chitosan and silk-fibroin blend for target-specific delivery of antitumor agents, Carbohydr Polym 277 (2022) 118862.

[43] M. Huang, Y. Pu, Y. Peng, Q. Fu, L. Guo, Y. Wu, Y. Zheng, Biotin and glucose dual-targeting, ligand-modified liposomes promote breast tumor-specific drug delivery, Bioorg Med Chem Lett 30(12) (2020) 127151.

[44] J. Su, F. Chen, V.L. Cryns, P.B. Messersmith, Catechol polymers for pH-responsive, targeted drug delivery to cancer cells, J Am Chem Soc 133(31) (2011) 11850-3.

[45] Z. Wang, B. Liu, Q. Sun, L. Feng, F. He, P. Yang, S. Gai, Z. Quan, J. Lin, Upconverted Metal-Organic Framework Janus Architecture for Near-Infrared and Ultrasound Co-Enhanced High Performance Tumor Therapy, ACS Nano 15(7) (2021) 12342-57.

[46] W. Yang, M. Wang, L. Ma, H. Li, L. Huang, Synthesis and characterization of biotin modified cholesteryl pullulan as a novel anticancer drug carrier, Carbohydr

Polym 99 (2014) 720-7.

[47] W. Feng, L. Chen, M. Qin, X. Zhou, Q. Zhang, Y. Miao, K. Qiu, Y. Zhang, C. He, Flower-like PEGylated MoS2 nanoflakes for near-infrared photothermal cancer therapy, Sci Rep 5 (2015) 17422.

[48] N. Lu, P. Huang, W. Fan, Z. Wang, Y. Liu, S. Wang, G. Zhang, J. Hu, W. Liu, G. Niu, R.D. Leapman, G. Lu, X. Chen, Tri-stimuli-responsive biodegradable theranostics for mild hyperthermia enhanced chemotherapy, Biomaterials 126 (2017) 39-48.

[49] X. Wu, W. Zhu, Stability enhancement of fluorophores for lighting up practical application in bioimaging, Chem Soc Rev 44(13) (2015) 4179-84.

[50] H. Zhao, J. Xu, C. Feng, J. Ren, L. Bao, Y. Zhao, W. Tao, Y. Zhao, X. Yang, Tailoring Aggregation Extent of Photosensitizers to Boost Phototherapy Potency for Eliciting Systemic Antitumor Immunity, Adv Mater 34(8) (2022) e2106390.

[51] Y. Ye, D.H. Bremner, H. Zhang, X. Chen, J. Lou, L.M. Zhu, Functionalized layered double hydroxide nanoparticles as an intelligent nanoplatform for synergistic photothermal therapy and chemotherapy of tumors, Colloids Surf B Biointerfaces 210 (2022) 112261.

[52] S. Ifuku, J.F. Kadla, Preparation of a Thermosensitive Highly Regioselective Cellulose/N-Isopropylacrylamide Copolymer through Atom Transfer Radical Polymerization, Biomacromolecules 9(11) (2008) 3308-3313.

[53] J. Zhang, Q. Wu, M.-C. Li, K. Song, X. Sun, S.-Y. Lee, T. Lei, Thermoresponsive Copolymer Poly(N-Vinylcaprolactam) Grafted Cellulose Nanocrystals: Synthesis,

Structure, and Properties, ACS Sustainable Chemistry & Engineering 5(8) (2017) 7439-7447.

[54] R. Pelton, Poly(N-isopropylacrylamide) (PNIPAM) is never hydrophobic, J Colloid Interface Sci 348(2) (2010) 673-4.

[55] R. Han, Q. Liu, Y. Lu, J. Peng, M. Pan, G. Wang, W. Chen, Y. Xiao, C. Yang, Z. Qian, Tumor microenvironment-responsive Ag2S-PAsp(DOX)-cRGD nanoparticles-mediated photochemotherapy enhances the immune response to tumor therapy, Biomaterials 281 (2022) 121328.

[56] J. Xu, Y. Xu, L. Sun, B. Lu, X. Yan, Z. Wang, T. Zhang, Glucose oxidase loaded Cu(2+) based metal-organic framework for glutathione depletion/reactive oxygen species elevation enhanced chemotherapy, Biomed Pharmacother 141 (2021) 111606.

Declaration of interests

☒ The authors declare that they have no known competing financial interests or personal relationships that could have appeared to influence the work reported in this paper.

☐ The authors declare the following financial interests/personal relationships which may be considered as potential competing interests:

.